Structural, electronic, and magnetic properties of pseudomorphic CrFe nanostripes on W(110)

T. Methfessel, M. Pratzer,* and H. J. Elmers†
Institut für Physik, Johannes Gutenberg-Universität Mainz, D-55128 Mainz, Germany
(Received 24 October 2006; revised manuscript received 22 February 2007; published 17 May 2007)

We have grown pseudomorphic binary $Cr_{1-x}Fe_x$ alloy monolayers and sequences of Cr and Fe nanostripes on W(110) by molecular-beam epitaxy in ultrahigh vacuum. By coadsorption of Cr and Fe a pseudomorphic random CrFe alloy grows on the W(110) substrate. At a substrate temperature of 700 K the CrFe alloy forms monolayer stripes in the step flow growth mode. We have measured magnetic properties of the monolayer alloy for $0.75 \leqslant x \leqslant 1$ using Kerr magnetometry. At a constant relative temperature $t=T/T_C$ the saturation value of the Kerr rotation shows a maximum at $x=0.95$ and then decreases with decreasing Fe concentration vanishing at $x=0.75$. The Curie temperature T_C shows a similar dependence on the composition. For $x \geqslant 0.75$ scanning tunneling spectroscopy reveals conductivity maxima in the unoccupied local density of states near the Fermi level at constant energies independent of the Cr concentration. This behavior can be explained by a simple model of *d*-band filling, similar to the explanation of the Slater-Pauling curve for binary alloys. We demonstrate the growth of artificially heterogeneous structures using sequential deposition of Fe and Cr. The temperature dependence of the multistripe growth and interdiffusion is investigated. Appropriate deposition parameters allow the growth of a two-dimensional analogon to an Fe-Cr-Fe spin valve.

DOI: 10.1103/PhysRevB.75.184419 PACS number(s): 75.70.Ak, 68.55.Nq, 75.50.Bb

I. INTRODUCTION

The increasing ability to prepare nanostructured materials on an atomic level has enormously extended the knowledge on the interplay of structure, electronic, and magnetic properties. As an example, the finding of an oscillating magnetic coupling between two ferromagnetic films separated by a nonferromagnetic interlayer of a few nanometer thickness[1,2] has not only rapidly led to a wide variety of applications including read heads of hard disks and sensors in automotive applications, but has also initiated the new research field of spin electronics.[3]

Within this field ultrathin epitaxial films have always played a leading role as a model case because of their well defined structure.[4] Single atomic layers grown on suitable substrates provide the unique possibility to determine structure and magnetic properties of all deposited material down to the atomic level.[5]

While the magnetic properties of pure element monolayers have been investigated to a considerable extent,[6,7] the magnetism of alloy monolayers and heterogeneous monolayers will provide new insights into the local ferromagnetic ordering mechanism.[8–11] Similar to bulk properties of binary alloys, the continuous variation of electronic and magnetic properties with the average number *N* of electrons per atom (Slater-Pauling curve)[12] might serve as a guideline for the prediction of properties of random alloy monolayers using the rigid-band model.[10,13–16] The prominent question is to what extent the magnetic and electronic properties of ultrathin films with a two-dimensional character can be described by similar models as used for bulk materials. Besides the deposition of homogeneous random alloy monolayers it is tempting to prepare well defined heterogeneous lateral structures,[17] i.e., a sequence of monolayer stripes of different elements offering the possibility of a microscopic lateral view on electronic coupling mechanisms.

Pseudomorphic (ps) $Co_{1-x}Fe_x$/W(110) monolayers showed a decreasing Curie temperature with decreasing Fe concentration, in contrast to the behavior of bulk alloys.[8–10] A phase separation of Co rich islands was observed only for high Co concentrations. Fe_xMn_{1-x} monolayers grow pseudomorphically and thermodynamically stable on W(110), too, independent of the alloy composition.[16] The Curie temperature and the Kerr rotation decreases with decreasing Fe concentration for Fe_xMn_{1-x}/W(110) monolayers. As supported by scanning tunneling spectroscopy these findings were explained by a simple model of *d*-band filling.[16]

We focus on the properties of pseudomorphic $Cr_{1-x}Fe_x$/W(110) monolayers for compositions $0.75 \leqslant x \leqslant 1.0$, covering the range of ferromagnetic alloy monolayers. Cr atoms possess two electrons less compared to Fe atoms thus allowing for a test of the simple model of *d*-band filling. We also investigate the possibility to grow heterogeneous nanostructures by sequential deposition of pure Fe and Cr monolayers. We demonstrate that a sequence of Fe-Cr-Fe multistripe can be grown starting at substrate step edges for appropriate deposition conditions, in close analogy to the Fe-Cr-Fe trilayer, the prototype of antiferromagnetic coupling investigations. The Cr monolayer provides an interesting interstripe since *ab initio* calculations predict an antiferromagnetic ground state for the Cr/W(110) monolayer.[18]

II. EXPERIMENT

The experiments were carried out in an ultrahigh vacuum chamber (UHV, $p < 1 \times 10^{-10}$ Torr) equipped with a four-grid low-energy electron diffraction (LEED) optics and an Omicron "Micro-STM" for measurements at room temperature. The single-crystal W(110) surface was cleaned by cycles of annealing in an oxygen atmosphere at 1200 K and subsequent flashing at 2000 K. As a consequence of the sample transfer, the thermocouple could not be fixed to the sample itself, but only to the sample holder. Consequently, absolute temperature values comprise a common error of about ±10 K. Therefore we calibrate absolute temperature

values for temperatures below room temperature by the Curie temperature of the elemental Fe monolayer [T_C(ML) =225 K],[6] thus conserving the smaller error of relative temperatures (±1 K).

For the preparation of random alloy monolayers we simultaneously deposited Fe and Cr (99.99% purity) from BeO crucibles with a rate of 0.1 ML/min at a substrate temperature of 300 K. After the deposition we annealed the samples at 700 K. Sequential deposition leading to heterogeneous monolayer structures was performed at various substrate temperatures as discussed below. The pressure increases during evaporation to $p=2\times10^{-10}$ Torr. The evaporation rate for both elements was monitored by a quartz balance which in turn was calibrated by scanning tunnel microscope (STM) images of pure element depositions covering approximately half of the substrate. The pseudomorphic growth of the first monolayer then enables an absolute determination of the deposited number of atoms. A pseudomorphic monolayer (ps-ML) corresponds to 0.82 bulk monolayers in the (110) plane both for Fe and Cr, because the almost equal bulk lattice constant for Fe and Cr is ≈9% smaller than the W lattice constant.

Magnetic properties were investigated in the preparation stage using Kerr magnetometry (wavelength of light 670 nm) as described in Ref. 6. Using a compensation technique, we measured the Kerr rotation in absolute units, as a function of temperature T and external field H. The external field was applied along [1$\bar{1}$0], i.e., along the easy axis.

Differential conductance dI/dU spectra were measured by scanning tunneling spectroscopy (STS), using a lock-in technique with a 8.44-kHz bias voltage modulation of 50 mV. All bias voltages denote sample voltages with respect to the tip. For STM and STS we have used a $Pt_{80}Ir_{20}$ tip cut under tensile stress from a thin wire.

III. GROWTH AND SCANNING TUNNELING SPECTROSCOPY OF RANDOM ALLOY MONOLAYERS

The growth of elemental Fe/W(110) (Ref. 19) and Cr/W(110) (Ref. 20) monolayers have been studied previously using STM. Both elements grow pseudomorphically on W(110) forming a (1×1) structure [for Cr/W(110) see Ref. 21]. While Fe grows in the step flow growth mode at elevated temperatures Cr was reported to form one-dimensional nanostructures.[20] A step flow growth mode was reported for the Cr monolayer on Mo(110).[22] From the fact that the Cr/W(110) system is similar to Cr/Mo(110) with respect to symmetry, misfit ($a_W-a_{Cr}/a_{Cr}=8.6\%$), and surface free energies $\gamma_{Cr}=2.3$ Jm^{-2}, $\gamma_W=3.3$ Jm^{-2}, one would expect a similar growth mode for the two elements and for the alloy as well.

In our study step flow growth has indeed been observed independent of the composition. Figure 1 shows the morphology of a $Cr_{0.3}Fe_{0.7}$/W(110) submonolayer deposited at $T=300$ K and after annealing at 700 K. The adsorbed monolayer forms continuous stripes attached to the substrate steps similar to the growth of elemental Fe. Because of the large

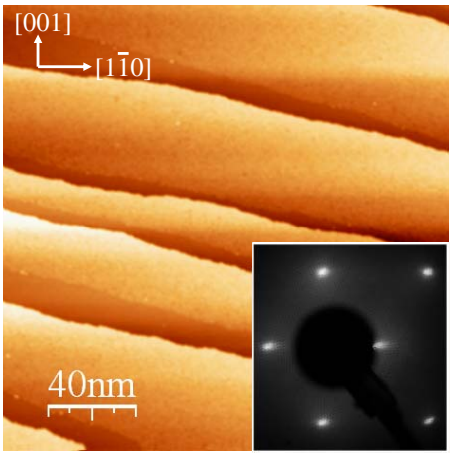

FIG. 1. (Color online) STM image (200×200 nm) of a $Cr_{0.3}Fe_{0.7}$/W(110) submonolayer film (coverage $\Theta=0.7$) deposited at 300 K and annealed at 700 K. The alloy monolayer appears at a larger topographic height (lighter color) than the bare W(110) surface. The LEED pattern ($E_i=80$ eV) shows a (1×1) pattern of a bcc(110) surface indicating the pseudomorphic growth. Tunneling parameters are $I=600$ pA, $U=1$ V.

free surface enthalpy of the W substrate, the monolayer is thermodynamically stable, i.e., islands of more than monolayer thickness do not appear even at higher annealing temperatures. From the homogeneous appearance of the adsorbed alloy layer we conclude that no phase separation takes place. The Fe and Cr atoms form a random alloy monolayer.

The LEED pattern (Fig. 1) shows a $p(1\times1)$ pattern. The absence of additional spots confirms the pseudomorphic structure of the adsorbed alloy monolayer. Similar LEED patterns were observed for compositions $0.5\leqslant x\leqslant0.9$. The LEED pattern is far from being similarly sharp as for the W(110) surface. This is not surprising, taking into account a chemical disorder for the random alloy. A $p(1\times1)$ pattern similarly sharp as for the W(110) surface appears for the pure element monolayers. From the LEED pattern we conclude that Fe and Cr atoms occupy exclusively regular W lattice sites.

In particular, we did not observe a $p(2\times1)$ or a $c(2\times2)$ superstructure for the Cr/W(110) monolayer, as would be expected for an antiferromagnetic order predicted by theory.[18] However, in our case the lowest possible temperature for LEED (150 K) is likely too high since we expect a lower Néel temperature. For the Fe/W(110) monolayer T_C(ML) is roughly a factor 5 smaller than the corresponding bulk value. Applying the same factor to the bulk Néel temperature of Cr (300 K) one would expect T_N(ML)=65 K for the Cr/W(110) monolayer.

The growth mode of alloy monolayers from island growth at room temperature to the step flow growth mode at 700 K is qualitatively similar for all compositions. However, the investigation of the submonolayer growth of elemental Cr reveals that Cr atoms exhibit a higher mobility on the W(110) surface at a given deposition temperature compared to Fe atoms. Cr forms monolayer islands with larger sizes than Fe at the same substrate temperature. On narrow ter-

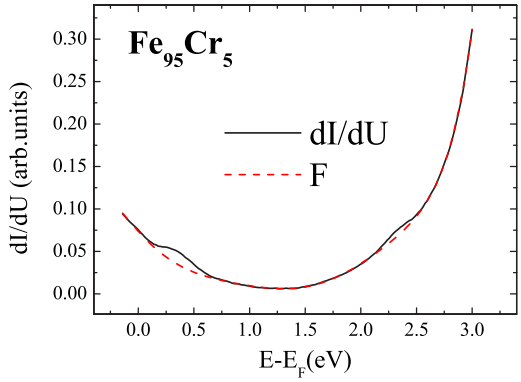

FIG. 2. (Color online) Differential conductivity (dI/dU) spectrum (full line) measured on ps-ML areas of $Cr_{0.05}Fe_{0.95}/W(110)$. Data shown result from an average of ≈10 individual spectra. The sample voltage modulation is 50 mV and the tip was stabilized at $U=0.7$ V and $I=600$ pA. The transmission function F is shown as a dashed (red) line.

races (<20 nm) Cr forms already stripes at room temperature (300 K). Contrarily, Fe grows in islands at this temperature.

The high mobility of Cr atoms on W(110) seems to be in disagreement with Ref. 20 reporting the formation of parallel plow furrows with a distance of 5 nm during growth of Cr on W(110) at room temperature. However, we observed a similar morphology as in Ref. 20 for the initial growth of Cr on a carbon contaminated W(110) surface. Carbon is a common contamination for W surfaces forming well-defined superstructures. It is likely that the C atoms act as nucleation centers for the Cr islands.

For the spectroscopic measurement we prepared a series of $Cr_{1-x}Fe_x/W(110)$ submonolayer films with a variation of the concentration in steps of $\Delta x=0.05$ in the range of $0.75 \leqslant x \leqslant 1$. The differential conductivity dI/dU was recorded on top of the pseudomorphic monolayer areas directly after preparation. The stabilization parameters ($U=+0.7$ V, $I=600$ pA), applied before the feedback loop was opened for measuring the tunneling spectra, were kept constant. These parameters determine the tip distance from the surface and strongly influence the relative peak heights, which might explain differences between our results and results reported previously.[16,23,24]

Spectra were measured with increasing sample bias starting at $U=-1$ V. A comparison of these data to spectra measured with decreasing voltage confirms that peak positions are not significantly shifted. In order to reduce the noise we averaged at least ten single spectra taken at random positions on each structure. This procedure also averages local variations of the electronic structure.

Figure 2 shows a dI/dU spectrum for $x=0.95$. The differential conductivity yields information on the local density of states (LDOS) of tip and sample. Assuming a constant density of states for the tip dI/dU might be approximated as $dI/dU \propto D_s(E_F)D_t(E_F+eU)F(eU-E_F)$. The smooth background function $F(eU-E_F)$ is mainly given by the tunneling transmission probability.[25] In order to correct the spectra for the transmission probability and emphasize the peak structure related to the local density of states the dI/dU spectra were normalized by $F(E-E_F)$ which in turn was determined by a fit to the experimental spectra outside the peak regions.

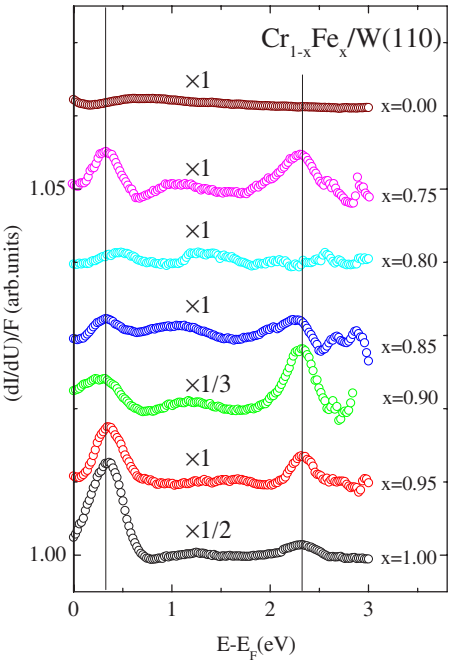

FIG. 3. (Color online) Differential conductivity (dI/dU) spectra (open circles) normalized to the voltage-dependent tunneling transmission function F, as obtained for pseudomorphic $Cr_{1-x}Fe_x/W(110)$ monolayers.

Figure 3 shows normalized spectra for $x=0$ and $0.75 \leqslant x \leqslant 1$. The tunneling spectra reveal significant variations for samples with only slightly varying composition. We attribute variations in the absolute dI/dU values and in the relative peak heights to different effective tip shapes and tip-samples distances.

For CrFe alloys with $0.75 \leqslant x \leqslant 1$ we observe peaks at $\Delta E=E-E_F=2.3$ eV and 0.3 eV for nearly all compositions. The data for $x=0.8$ represent an exception. Weak peaks occur at $\Delta E=E-E_F=0.5$ and 1.5 eV, while the peak at 2.3 eV is absent. We assume that this is an experimental artifact due to contamination.

The peaks at 0.3 and 2.3 eV are emphasized in Fig. 3 by the vertical lines. Both peaks were observed previously for the elemental Fe/W(110) monolayer[16,23] and also for the Fe/Mo(110) monolayer[26] at a slightly higher energy (0.4 eV). Since the peaks do not shift with composition their origin is likely similarly independent of x. The observation of peaks at constant energetic positions is in contrast to the continuous shift towards lower energies with decreasing Fe concentration observed for $Fe_xMn_{1-x}/W(110)$.[16]

The peak at 2.3 eV might be attributed to a flat d-band structure calculated at 2.2 eV,[27,28] both for minority and majority electrons. The peak at 0.3 eV is characteristic for the Fe(110) monolayer since it was observed both for Fe/Mo(110) and Fe/W(110) and also for various tip materials.[16,23,26] However, *ab initio* calculations do not indicate a high density of states value at 0.3 eV, but instead a prominent double peak structure at $0.8<\Delta E<1.4$ eV,[27,28] which was not observed in our experiment.

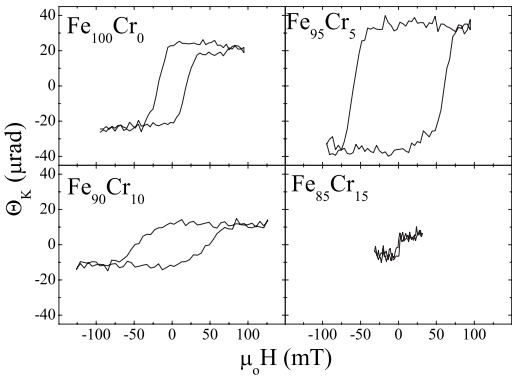

FIG. 4. Magnetization loops measured for $Cr_{1-x}Fe_x/W(110)$ submonolayer films ($\Theta=0.7$ ML) at $T/T_C(\mathrm{ML})=0.9$. For $x<0.85$ no Kerr signal was detected.

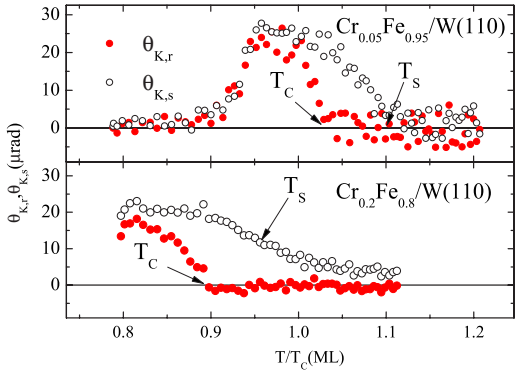

FIG. 5. (Color online) Dependence of the remnant and saturation Kerr rotation, $\theta_{K,r}$ and $\theta_{K,s}$, on temperature for a $Cr_{0.8}Fe_{0.2}/W(110)$ submonolayer film ($\Theta=0.7$ ML).

The spectrum of the elemental Cr monolayer on W(110) shown for comparison in Fig. 3 strongly deviates from the spectra observed for the Fe rich CrFe alloy monolayer. A broad maximum appears at 0.7 eV while the conductivity is low at the previous maxima.

IV. MAGNETIC PROPERTIES OF RANDOM ALLOY MONOLAYERS

Using Kerr magnetometry we measured hysteresis loops after the samples have been cooled down to 155 K. A series of magnetization loops was measured without active cooling during slowly warming up in order to avoid pumping vibrations. The temperature changes during one loop by only 5 K. Except close to T_C the magnetic properties will not change severely in this temperature range. Figure 4 compares loops for $Cr_{1-x}Fe_x/W(110)$ submonolayer films with a constant coverage of $\Theta=0.7$ ML and at a constant relative temperature of $T/T_C(\mathrm{ML})=0.9$.

The coverage $\Theta=0.7$ ML avoids the formation of double layer areas. On the other hand, it is large enough to certify that laterally averaged magnetic properties are nearly independent of the coverage.[6] STM images reveal a large variation of terrace widths from 10 to 200 nm although the W surface was polished with an accuracy of 0.1°, which is typical for W crystals.[6] As a consequence, some nanostripes are narrower than 10 nm. Their lower Curie temperature broadens the observed phase transition. However, the area comprising these very narrow terraces is quite small. The average terrace width is about 40 nm.

At a relative temperature of $T/T_C(\mathrm{ML})=0.9$ a nonzero magnetization signal can be observed for $x\geqslant 0.85$. For all compositions we observe easy axis loops at low temperatures, i.e., the remnance signal equals the saturation signal. This observation confirms that the easy axis is parallel to $[1\bar{1}0]$, similar as for $Co_{1-x}Fe_x/W(110)$ and $Fe_xMn_{1-x}/W(110)$ monolayers. At $T/T_C(\mathrm{ML})=0.9$ the coercive field and the Kerr rotation angle $\theta_{K,s}$ at saturation increase from $x=1$ to $x=0.95$ and decrease again with further increase of the Cr concentration. This is likely indicative for a maximum of the magnetization at $x=0.95$ since the magnetooptical constants typically vary only slightly with composition. The maximum of the Kerr rotation persists at higher temperatures. Below $T/T_C(\mathrm{ML})=0.9$ the coercive force exceeds our maximum available field for $x=0.95$ thus prohibiting a measurement of the Kerr signal at lower temperatures.

Temperature-dependent data for the remnant and saturation Kerr rotation, $\theta_{K,r}$ and $\theta_{K,s}$, were obtained using a four-point measurement of $\theta_{K,r}$ and $\theta_{K,s}$ from data taken at $H=+H_{max}$, $H=0$, $H=-H_{max}$, and $H=0$ with $\mu_0 H_{max}=0.1$ T. Thus the temperature resolution could be significantly increased. As shown in Fig. 5 for $x=0.8$ and $x=0.95$, the remnant signal vanishes at the Curie temperatures $T/T_C(\mathrm{ML})=0.89$ and $T/T_C(\mathrm{ML})=1.03$, while the saturation signal measured at $\mu_0 H=0.1$ T could be detected at still higher temperatures. The saturation signal does not approach zero but a constant positive value. We define a critical temperature T_s indicative for the loss of the saturation signal at the inclination point of $\theta_{K,s}(T)$. For $Cr_{0.2}Fe_{0.8}/W(110)$ we thus obtain $T_s/T_C(\mathrm{ML})=0.95$.

Vanishing longitudinal signals could be due to a change of the easy axis from the in-plane $[1\bar{1}0]$ direction to the out-of-plane [110] direction. If such a spin reorientation of the easy axis with increasing Cr concentration were present one would expect a gradual change from easy axis loops to hard axis loops, which was not observed. Moreover, the magnetic crystal anisotropy of the Fe monolayer supporting the shape anisotropy with in-plane easy axis is very large.[30] Therefore we assume that the easy axis remains in-plane for all compositions.

Figure 6 summarizes values of T_C and T_s obtained for various compositions. The Curie temperature T_C and the critical temperature T_s show a maximum for $x=0.95$ and then decreases with further increasing Cr concentration. The decreasing rate of the Curie temperature with increasing Cr concentration $[\Delta T_C(x)/\Delta x]/T_C(\mathrm{ML})=-(1.3\pm0.2)\times10^{-2}$ is smaller than the rate of -1.8×10^{-2} observed for $Mn_{1-x}Fe_x/W(110)$. The overall composition dependence of $T_C(x)$ is surprisingly similar to the bulk behavior of the corresponding binary CrFe alloy.[29]

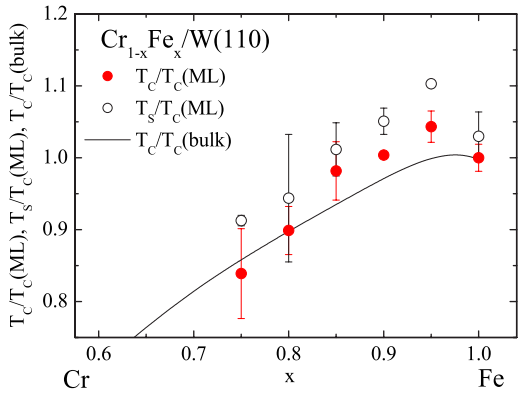

FIG. 6. (Color online) Dependence of the Curie temperature T_C on the alloy composition of a $Cr_{1-x}Fe_x$ submonolayer ($\Theta=0.7$). Bulk values (Ref. 29) are shown for comparison.

V. GROWTH OF HETEROGENEOUS MONOLAYER STRUCTURES

Heterogeneous lateral structures were prepared by sequential deposition of the elements Fe and Cr in analogy to the preparation of multilayers. We first deposited an Fe coverage of 0.3 ps-ML at a substrate temperature of 700 K. Fe monolayer stripes grow starting at the W substrate steps. After cooling down to 300 K we deposited 0.3 ps-ML Cr.

The topography observed by STM (Fig. 7) clearly shows two adjacent monolayer stripes with a well defined boundary between them. For the STM image we have chosen an area with exceptionally narrow terrace widths. The limited mobility of adsorbed atoms at a deposition temperature of 300 K leads to island formation on wider terraces. However, comparing the growth of Fe and Cr on W(110), the mobility of Cr is much higher at room temperature compared to that of Fe.

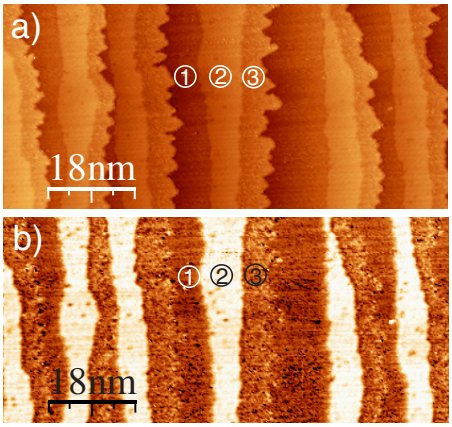

FIG. 7. (Color online) (80×40) nm^2 STM (a) and STS images (b) of a sequentially deposited double stripe of Fe (0.3 ML) deposited at $T=700$ K and Cr (0.3 ML) at $T=300$ K on W(110) ($U=0.24$ V, $I=0.55$ nA). Marks denote the distinct areas of the bare substrate (1), the Fe stripe next to the substrate edge (2), and the Cr stripe (3) comprising a topographical step at the right side. Crystallographic low-index directions point along the vertical [001] and horizontal $[1\bar{1}0]$ directions.

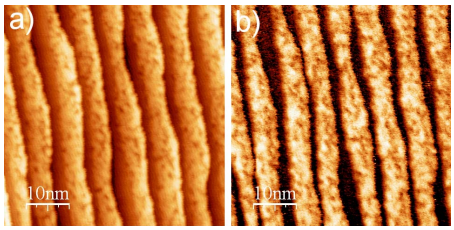

FIG. 8. (Color online) (50×50) nm^2 STM (a) and STS images (b) of a sequentially deposited double stripe of Fe (0.3 ML) deposited at $T=700$ K and Cr (0.3 ML) at $T=300$ K on W(110) ($U=0.24$ V, $I=0.55$ nA) after annealing at 560 K. Crystallographic low-index directions point along the vertical [001] and horizontal $[1\bar{1}0]$ directions.

From the sequence of deposition it is obvious that the left stripes next to the step consists of Fe while the right stripes consist of Cr. On the topographical image the Fe stripes appear with a larger height than the Cr stripes. This effect can also reflect differences in the electronic structure. The dI/dU map measured simultaneously reveals a higher conductivity on the Fe stripe compared to the bare W substrate and the Cr stripe. This is in agreement with the peak observed at +0.3 eV in the Fe spectra (see Fig. 3).

Because the Cr stripe was deposited at lower temperature the stripe edge appears not very smooth and shows instead a pronounced meandric structure. This corresponds to an island growth occurring for three-dimensional growth. In an attempt to straighten the step edge we annealed samples as shown in Fig. 7 to higher temperatures. Up to $T=500$ K we did not observe any morphological changes. An annealing temperature of 560 K, however, already leads to a noticeable interdiffusion of Cr and Fe as shown in Fig. 8. At this annealing temperature an inhomogeneous monolayer has formed with brighter and darker areas. The brighter areas of the monolayer, indicating a larger height in the topographical image and higher conductivity in the spectroscopic image, might be attributed to Fe areas in agreement with Fig. 7. The bright areas cover more than the expected half of the nanostripe area. The domination of the bright areas might result from the fact that the dI/dU spectra of a $Cr_{1-x}Fe_x$ monolayer shows a peak at +0.3 eV for a range of compositions $1\leqslant x\leqslant0.25$ (see Fig. 3). Thus the bright areas indicate not only pure Fe regions but also Fe-rich $Cr_{1-x}Fe_x$ monolayer areas.

Figure 9 shows the result of sequential deposition in reversed order compared to Fig. 7, i.e., the Cr stripe was deposited first. The second deposited Fe forms noncontinuous stripes at the low deposition temperature of 300 K. Both the topographical and the conductivity map reveal a contrast at the boundaries between them. In the topographical image the Cr stripe appears slightly relaxed downwards with respect to the W(110) layer distance, while the Fe monolayer shows a larger height. A quantitative evaluation of the tip height difference results in a downward relaxation of $-10\pm2\%$ for Cr and $+10\pm2\%$ for Fe both measured relative to the W(110) layer distance.

Minimization of total energies in an *ab initio* study predicted a relaxation of the Cr-W layer distance with respect to the bulk W(110) layer distance of -16% (Ref. 18) for the

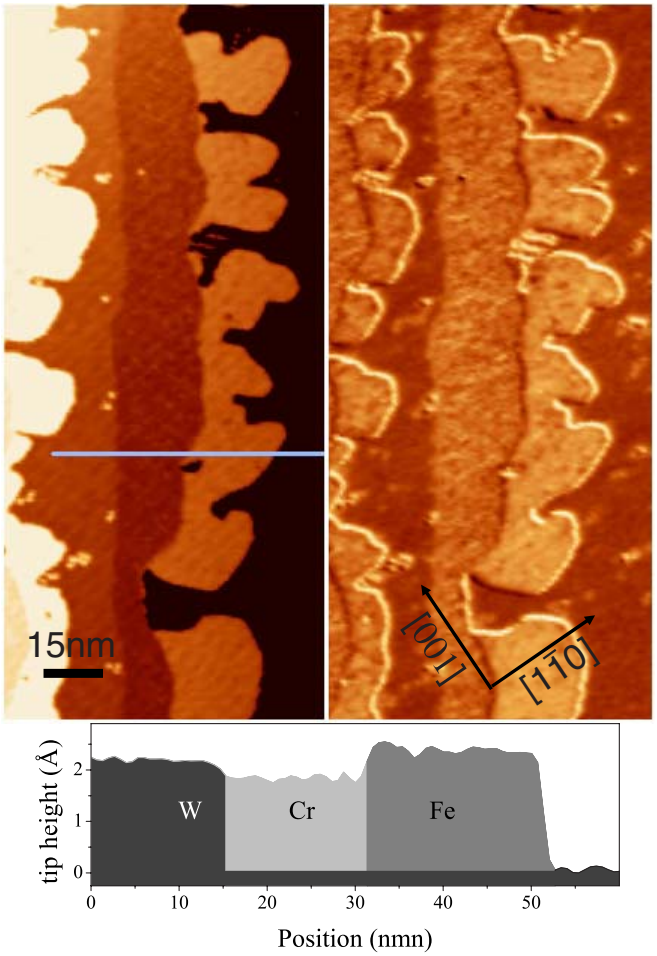

FIG. 9. (Color online) (180×70) nm^2 STM (a) and STS images (b) of a sequentially deposited double stripe of first Cr (0.3 ML) deposited at T=700 K and then Fe (0.3 ML) at T=300 K on W(110) (U=0.44 V, I=0.6 nA). Marks denote the distinct areas of the bare substrate (1), the Cr stripe next to the substrate edge (2), and the Fe stripe (3) comprising a topographical step at the right side. (c) Topographical profile along the line indicated in (a). Positions of Fe and Cr stripes are indicated.

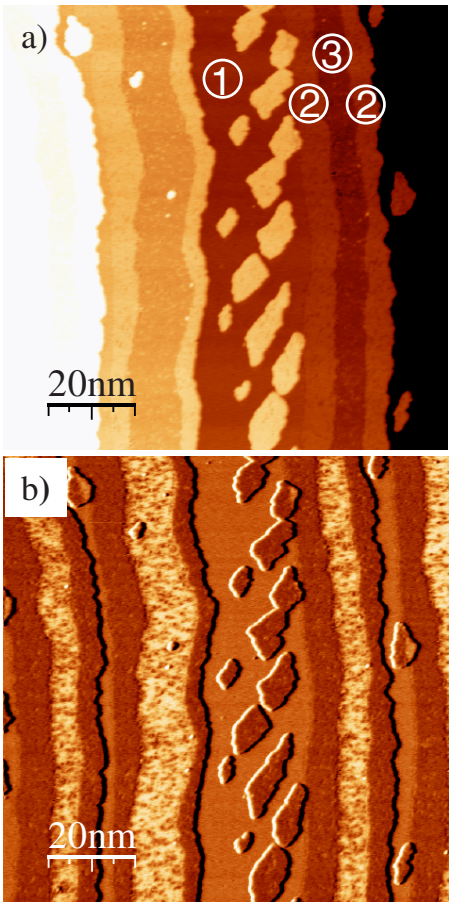

FIG. 10. (Color online) (100×100) nm^2 STM (a) and STS images (b) of a sequentially deposited triple stripe of Fe (0.3 ML) deposited at T=700 K and Cr (0.3 ML) at T=500 K and a second Fe stripe at T=340 K on W(110) (U=0.24 V, I=0.55 nA). Marks denote areas of the bare substrate (1), the two Fe stripes (2), and the intermediate Cr stripe (3). Crystallographic low-index directions point along the vertical [001] and horizontal [1$\bar{1}$0] directions.

nonmagnetic state, −14% for a $p(2\times1)$ antiferromagnet, and −10% for the $p(2\times1)$ antiferromagnet with the lowest total energy. A reduction of −13% of the Fe-W layer distance was found from a combined experimental and theoretical investigation of LEED intensities for Fe/W(110).[31]

In our experiment the Cr-W distance appears considerably smaller than the Fe-W distance. Assuming that the integrated conductivity for Fe/W(110) is similar to Cr/W(110) this difference might reflect at least partly a true topographical difference. In the theoretical results a smaller relaxation for Fe than for Cr occurs only for the case of a nonmagnetic Cr state. Therefore one might infer that the Cr monolayer is in the nonmagnetic state. However, one should keep in mind that STM measures a convolution of actual layer height and differences in the integrated dI/dU value.

For the preparation of triple Fe-Cr-Fe stripes, we increased the deposition temperature of the Cr stripe just below the interdiffusion temperature to avoid island formation on wider terraces. Figure 10 shows an example of a triple stripe where we sequentially deposited an Fe stripe (0.2 ML) at T=700 K, a Cr stripe (0.3 ML) at T=500 K, and finally again an Fe stripe (0.2 ML) at T=340 K. The three stripes can be easily distinguished in the dI/dU map. A clear boundary between the stripes indicates that a massive interdiffusion has been avoided. Moreover, the observed coverage corresponds to the deposited material. The increased substrate temperature during the Cr deposition step clearly leads to a straighter boundary between the Cr stripe and the second Fe stripe. The temperature during the deposition of the second Fe layer was further reduced in order to inhibit an incorporation of Fe atoms into the Cr layer. Possibly this could not fully be avoided as concluded from the inhomogeneous dI/dU signal within the Cr interstripe. The low deposition temperature leads to the creation of islands on the wider terraces. A few double layer islands show up on the center terrace. The island growth can be avoided at a higher deposition temperature on the expense of an increased interdiffusion.

The change of the tip height across the triple stripe is in agreement with the double stripe systems shown in Figs. 7 and 9. The Cr monolayer appears lower than the Fe mono-

layer. This again confirms the formation of a triple stripe system with the intended sequence of stripes.

Surprising is the change of the spectroscopic contrast: While in Figs. 7 and 9, Cr stripes appear darker (lower dI/dU value) than Fe stripes, Fig. 10 shows a reversed contrast. A similar reversed contrast appeared for lower Cr deposition temperature. In this case Cr islands are surrounded by a rim of lower conductivity caused by the Fe monolayer deposited in the third deposition step again at 340 K. The change of the conductivity may be caused either by interdiffusion or by residual gas contamination, i.e., adsorption of carbon monoxide or hydrogen. Adsorption of residual gases is not unlikely since Cr appears particularly reactive. On the other hand, in the case of Fig. 10 the third stripe was deposited at 340 K instead of 300 K, which might increase the mobility of Cr atoms considerably and allow for an inclusion of few isolated Fe atoms adsorbed on the Cr layer in the third deposition step. The Fe impurities might change the local conductivity very efficiently, while the topographical height remains constant.

VI. CONCLUSION

In contrast to experimental results for random FeMn and CoFe alloy monolayers we observed prominent peaks in the dI/dU spectra at constant energy values, indicating that electronic states are not shifted with increasing Cr concentration in the alloy monolayer.

This is surprising at first glance because Cr has two d-electrons less than Fe. Considering a rigid-band model one would expect a decrease of the mean number of electrons in d bands with increasing Cr concentration. Counting exclusively d electrons would result in a reduction of d electrons twice as much as for Mn for a given concentration. According to the rigid-band model the reduction of d electrons would result in a decrease of the Fermi energy. Because the Fermi energy defines the zero point on our energy scale one expects a shift of the prominent peaks towards higher energy.

In the case of FeMn a shift in the opposite direction occurred, indicating an effect that was already predicted by Friedel,[32] namely an emptying of the occupied 4s states of Mn into the d states of the alloy. The 4s electrons of Mn thus overcompensated the reduction of the initial number of d electrons.

Adopting the same consideration to the present case of CrFe alloys, the mean number of original d electrons is decreased by $\Delta N'_{3d}=c\Delta Z$ with increasing concentration c because of the difference of the atomic number of Cr and Fe $\Delta Z=-2$. The total number of the original Cr 4s electrons that can be emptied into the d electron sea is given by $\Delta N'_{4s}=2c$. For the case of Cr one obtains a total change of the number of d electrons of $\Delta N_{3d}=c(2+\Delta Z)=0$. The number of Cr 4$s$ electrons and the lack of 2d electrons compensate each other. This consideration predicts a constant level of d-electron states for CrFe alloys while MnFe alloys should show a decrease of the peak positions with respect to the Fermi energy. Thus the prediction is in nice agreement with the experimental observation.

For the case of $Co_{1-x}Fe_x/W(110)$ and $Mn_{1-x}Fe_x/W(110)$ monolayers the decrease of the peak positions of unoccupied states towards the Fermi edge was related to a decrease of T_C. In the case of $Cr_{1-x}Fe_x/W(110)$ the peak positions remain constant and one would expect a constant T_C. Indeed, we observe an almost constant value for T_C at least for very small Cr concentrations. This is in contrast to the case of $Co_{1-x}Fe_x/W(110)$ and $Mn_{1-x}Fe_x/W(110)$ where T_C decreases linearly with increasing Mn or Co concentration.

The rigid-band model is a very crude approximation of the change of electronic states in alloys. It may serve as a rough guideline only. Progress of computational power will allow future band-structure calculation that can explain the observed features in more detail. Nevertheless, it will be very interesting to investigate the case of $V_{1-x}Fe_x/W(110)$ alloy monolayer where a shift of the peak positions in the direction of higher energies is expected.

A measurement of the magnetic properties of the heterogeneous multistripe system would be quite interesting. The large variation of the stripe widths, which is due to the variation of the terrace width, likely causes a compensation of local exchange coupling effects by averaging if nonlocal probes are applied.

In summary, pseudomorphic $Cr_{1-x}Fe_x/W(110)$ binary alloy monolayers show characteristic maxima in the local density of states independent of the alloy composition. For small Cr concentrations this effect is related to an almost constant value of T_C. For higher Cr concentrations T_C decreases similar to the behavior of bulk alloys. A sequential deposition method for the preparation of artificially structured two-dimensional magnetic systems has been demonstrated.

ACKNOWLEDGMENT

We thank the Deutsche Forschungsgemeinschaft for financial support.

*Present address: 2. Physikalisches Institut B, RWTH-Aachen, D-52074 Aachen, Germany.

†Email address: elmers@uni-mainz.de

[1] P. Grünberg, R. Schreiber, Y. Pang, M. B. Brodsky, and H. Sowers, Phys. Rev. Lett. **57**, 2442 (1986).

[2] M. N. Baibich, J. M. Broto, A. Fert, F. Nguyen Van Dau, F. Petroff, P. Etienne, G. Creuzet, A. Friederich, and J. Chazelas, Phys. Rev. Lett. **61**, 2472 (1988).

[3] G. A. Prinz, Science **282**, 1660 (1998).

[4] U. Gradmann, in *Handbook of Ferromagnetic Materials*, edited by K. H. J. Buschow (Elsevier, Amsterdam, 1993), Vol. 7, p. 11.

[5] M. Bode, S. Heinze, A. Kubetzka, O. Pietzsch, M. Hennefarth,

M. Getzlaff, R. Wiesendanger, X. Nie, G. Bihlmayer, and S. Blügel, Phys. Rev. B **66**, 014425 (2002).
[6] H. J. Elmers, Int. J. Mod. Phys. B **9**, 3115 (1995).
[7] M. Bode, M. Hennefarth, D. Haude, M. Getzlaff, and R. Wiesendanger, Surf. Sci. **432**, 8 (1999).
[8] J. P. Pierce, E. W. Plummer, and J. Shen, Appl. Phys. Lett. **81**, 1890 (2002).
[9] M. Pratzer and H. J. Elmers, Phys. Rev. Lett. **90**, 077201 (2003).
[10] D. Spisak and J. Hafner, Phys. Rev. B **70**, 014430 (2004).
[11] Z. W. Zhou, Q. Y. Li, and D. Venus, J. Appl. Phys. **99**, 08N504 (2006).
[12] S. Chikazumi, *Physics of Ferromagnetism* (Clarendon Press, Oxford, 1997).
[13] F. O. Schumann, R. F. Willis, K. G. Goodman, and J. G. Tobin, Phys. Rev. Lett. **79**, 5166 (1997).
[14] A. Dittschar, W. Kuch, M. Zharnikov, and C. M. Schneider, J. Magn. Magn. Mater. **212**, 307 (2000).
[15] F. Matthes, M. Seider, and C. M. Schneider, J. Appl. Phys. **91**, 8144 (2002).
[16] M. Pratzer and H. J. Elmers, Phys. Rev. B **69**, 134418 (2004); J. Magn. Magn. Mater. **272**, 1201 (2004).
[17] P. Gambardella, M. Blanc, K. Kuhnke, K. Kern, F. Picaud, C. Ramseyer, C. Girardet, C. Barreteau, D. Spanjaard, and M. C. Desjonqueres, Phys. Rev. B **64**, 045404 (2001).
[18] X. Wei, P. Jiang, and J. G. Che, Chin. Phys. Lett. **22**, 1232 (2005).
[19] H. Bethge, D. Heuer, C. Jensen, K. Reshöft, and U. Köhler, Surf. Sci. **331–333**, 878 (1995).
[20] E.-P. Kim, T.-H. Kim, S.-T. Kim, Y. Kuk, and S.-J. Kahng, Thin Solid Films **441**, 317 (2003).
[21] P. J. Berlowitz and D. N. Shinn, Surf. Sci. **209**, 345 (1989).
[22] A. Cazacu, S. Murphy, and I. V. Shvets, Phys. Rev. B **73**, 045413 (2006).
[23] M. Bode, A. Kubetzka, O. Pietzsch, and R. Wiesendanger, Surf. Sci. **513**, 135 (2002).
[24] O. Pietzsch, A. Kubetzka, M. Bode, and R. Wiesendanger, Phys. Rev. Lett. **84**, 5212 (2000).
[25] V. A. Ukraintsev, Phys. Rev. B **53**, 11176 (1996).
[26] J. Prokop, A. Kukunin, and H. J. Elmers, Phys. Rev. B **73**, 014428 (2006).
[27] X. Qian and W. Hübner, Phys. Rev. B **60**, 16192 (1999); **67**, 184414 (2003).
[28] T.-H. Rho, Gi-B. Cha, Y. Kwon, C. Lee, and S.-C. Hong, J. Korean Phys. Soc. **35**, 564 (1999).
[29] T. Nishizawa and K. Ishida, *Binary Alloy Phase Diagrams* (ASM, Materials Park, OH, 1986); M. Hansen and K. Anderko, *Constitution of Binary Alloys* (McGraw-Hill, New York, 1958).
[30] M. Pratzer, H. J. Elmers, M. Bode, O. Pietzsch, A. Kubetzka, and R. Wiesendanger, Phys. Rev. Lett. **87**, 127201 (2001).
[31] M. Albrecht, U. Gradmann, Th. Reichert, and L. Fritsche, Solid State Commun. **78**, 671 (1991).
[32] J. Friedel, J. Phys. Radium **23**, 501 (1962); **23**, 692 (1962).